catalysts

MDPI

Article

Heterogeneous Photo-Fenton Degradation of Azo Dyes over a Magnetite-Based Catalyst: Kinetic and Thermodynamic Studies

Jackson Anderson S. Ribeiro [1], Júlia F. Alves [1], Bruno César B. Salgado [2], Alcineia C. Oliveira [3], Rinaldo S. Araújo [1,*] and Enrique Rodríguez-Castellón [4,*]

[1] Departamento de Química e Meio Ambiente, Instituto Federal de Educação-IFCE, Campus de Fortaleza, Av. 13 de Maio, Fortaleza 60040-531, CE, Brazil; jacksons.anderson.sena07@aluno.ifce.edu.br (J.A.S.R.); julia.ferreira.alves08@aluno.ifce.edu.br (J.F.A.)
[2] Departamento de Química e Meio Ambiente, Instituto Federal de Educação-IFCE, Campus de Maracanaú, Av. Parque Central, Maracanaú 61939-140, CE, Brazil; brunocesar@ifce.edu.br
[3] Departamento de Química Analítica e Físico-Química, Universidade Federal do Ceará, Campus do Pici, Bloco 940, Fortaleza 60455-760, CE, Brazil; alcineia@ufc.br
[4] Departamento de Química Inorgánica, Instituto Interuniversitario de Investigación en Biorrefinerías I3B, Facultad de Ciencias, Universidad de Málaga, 29071 Málaga, Spain
* Correspondence: rinaldo@ifce.edu.br (R.S.A.); castellon@uma.es (E.R.-C.)

Abstract: Textile wastewater containing dyes poses significant environmental hazards. Advanced oxidative processes, especially the heterogeneous photo-Fenton process, are effective in degrading a wide range of contaminants due to high conversion rates and ease of catalyst recovery. This study evaluates the heterogeneous photodegradation of the azo dyes Acid Red 18 (AR18), Acid Red 66 (AR66), and Orange 2 (OR2) using magnetite as a catalyst. The magnetic catalyst was synthesized via a hydrothermal process at 150 °C. Experiments were conducted at room temperature, investigating the effect of catalyst dosage, pH, and initial concentrations of H_2O_2 and AR18 dye. Kinetic and thermodynamic studies were performed at 25, 40, and 60 °C for the three azo dyes (AR18, AR66, and OR2) and the effect of the dye structures on the degradation efficiency was investigated. At 25 °C for 0.33 mmolL^{-1} of dye at pH 3.0, using 1.4 gL^{-1} of the catalyst and 60 mgL^{-1} of H_2O_2 under UV radiation of 16.7 mWcm^{-2}, the catalyst showed 62.3% degradation for AR18, 79.6% for AR66, and 83.8% for OR2 in 180 min of reaction. The oxidation of azo dyes under these conditions is spontaneous and endothermic. The pseudo-first-order kinetic constants indicated a strong temperature dependence with an order of reactivity of the type OR2 > AR66 > AR18, which is associated with the molecular size, steric hindrance, aromatic conjugation, electrostatic repulsion, and nature of the acid–base interactions on the catalytic surface.

Keywords: heterogeneous photo-Fenton-like; magnetite; degradation; azo dyes; molecular effects

Citation: Ribeiro, J.A.S.; Alves, J.F.; Salgado, B.C.B.; Oliveira, A.C.; Araújo, R.S.; Rodríguez-Castellón, E. Heterogeneous Photo-Fenton Degradation of Azo Dyes over a Magnetite-Based Catalyst: Kinetic and Thermodynamic Studies. *Catalysts* **2024**, *14*, 591. https://doi.org/10.3390/catal14090591

Academic Editor: Elisabete C.B.A. Alegria

Received: 6 August 2024
Revised: 30 August 2024
Accepted: 31 August 2024
Published: 3 September 2024

1. Introduction

Due to environmental concerns, the global demand for lesser consumption of water and lower discharge of industrial and domestic wastewater is a major challenge to environmental sustainability [1,2]. An important example is the consumption of excessive amounts of water and synthetic dyes by textile industrial processes, which have harmful effects on human health and ecosystems, resulting in a huge amount of non-biodegradable organic compounds in the environment [2–4]. In this respect, hazardous wastewater treatment processes for removing organic pollutants are required to overcome their excess and improve the quality of discharged water.

Efficient processes for the rapid removal of organic contaminants, such as the use of advanced oxidation processes (AOPs), have become ubiquitous in remediation methods for the clean-up of wastewater by organic contaminant degradation to mitigate their adverse consequences on the environment [5,6]. Moreover, the state-of-the-art in AOPs

shows the chemical oxidation of dyes through in situ generation of highly reactive oxygen species, e.g., hydroxyl radicals ($^{\bullet}OH$), superoxide radicals ($O_2^{\bullet-}$), and singlet oxygen ($^1O_2$), by mechanistic routes of photocatalysis, ozonation, electrocatalysis, oxidation by the Fenton reaction, and Fenton-like processes [7–11]. One of the promising routes for dye degradation is the homogeneous or heterogeneous Fenton process, which has outstanding advantages for textile wastewater removal with a rapid reaction rate and time [7,12,13]. As a heterogeneous reaction, the photo-Fenton-like processes hold the advantages of using no light to degrade contaminants and recovering and recycling the catalyst from the reaction medium more efficiently than other dye degradation processes [13–15].

One of the difficulties associated with the utilization of benchmark photo-Fenton catalysts such as α-Fe_2O_3, Fe_3O_4, and FeOOH, among other iron-based oxides, is a high photogenerated electron–hole pair complexation rate, which is considered a crucial factor that influences the low accessibility of the active sites and the light absorption efficiency of the catalytic performance in these processes [15–17]. In addition, the use of other iron-based materials such as ash can efficiently be considered for Fenton-like reactions [18].

It is acknowledged that the current state of Fe^{2+} ions present in magnetite is not yet sufficient to reliably assign H_2O_2, given the aforementioned hydroxyl and hydroperoxyl radical ($HO_2^{\bullet}$) and/or superoxide radical anions [15–17]. The magnetite-holding spinel structure allows the oxidation of its Fe^{2+} sites to Fe^{3+} sites, along with the consumption of $^{\bullet}OH$ radicals by the proper Fe^{2+} ion, producing high efficiencies for oxidizing organic pollutants [19].

On the other hand, it should be noted that the use of magnetite as a catalyst allows the unit operation to be reduced and accelerates the recovery of the magnetic catalyst, which makes wastewater treatment more inexpensive. The improvement of magnetite's properties seems to be very promising for obtaining a highly stable catalyst during reactions for the oxidative degradation of dyes at circumneutral pH [15,17].

Therefore, it is considered important to understand magnetite's properties to optimize the catalyst's activity in the heterogeneous photo-Fenton-like process for the oxidation of azo dyes; however, the effect of functional groups present in the dye molecule during the heterogeneous phase of oxidation has been little explored in the literature.

In the present study, the effects of H_2O_2, pollutant concentration, pH, and the amount of catalyst on the degradation of the azo dye Acid Red 18 (AR18) were examined, along with the kinetics and thermodynamics of degradation. This study aims to explore the relationship between dye behavior and the photodegradation characteristics for the oxidation of azo molecules such as Orange 2 (OR2), Acid Red 66 (AR66), and AR18 itself.

2. Results and Discussion

2.1. Heterogeneous Photo-Fenton-Like Reaction

Figure 1 shows the photodegradation performance of the AR18 azo dye over the Fe_3O_4 catalyst. The effects of catalyst dosage in the Heterogeneous Fenton-like reaction on the degradation efficiency of the AR18 azo dye compared with other reaction systems are investigated.

Preliminary catalytic runs to analyze the catalyst dosage variations on the efficient degradation of AR18 over a magnetite catalyst are shown in Figure 1a. It may be noted that the AR18 degradation slightly increases from 58 to 88% from a catalyst dosage of 0.5 to 1.4 gL^{-1}, when using an initial AR18 of ca. 60 mgL^{-1} within 120 min. However, degradation at 2.0 gL^{-1} slightly decreases, achieving 83%. The enhancement in degradation efficiency may be attributed to the combined effects of direct oxidation by UV light (photolytic mechanism) and the contribution of this radiation to the formation of $^{\bullet}OH$ radicals via decomposition of H_2O_2 in an aqueous medium (photochemical mechanism) and/or on the surface of the catalyst (photocatalytic mechanism), according to Equations (1) to (3). On the other hand, the slight reduction in catalytic activity for a dosage of 2.0 gL^{-1} may be associated with difficulty in penetrating light into the reaction medium due to the amount

of the catalyst in suspension. Nevertheless, such a rapid drop in percentage degradation is not reflected in any alteration of the magnetite structure.

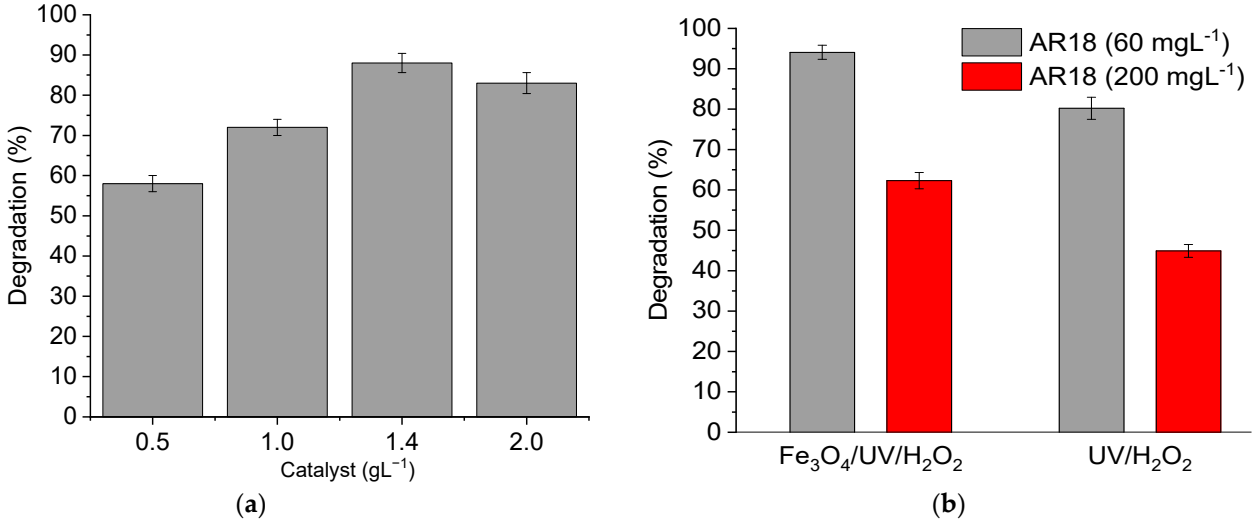

Figure 1. Effects of AR18 degradation at 25 °C with I_L = 16.7 mWcm^{-2}. (**a**) Initial catalyst dosage using a C_0(AR18) of ca. 60 mgL^{-1} and C_0(H_2O_2) of ca. 30 mgL^{-1} at a pH of 3.0 during 120 min of reaction time. (**b**) Blank runs of the degradation of AR18 over magnetite in distinct reaction conditions. C_0(Fe_3O_4) = 1.4 gL^{-1}, C_0(AR18) = 60 mgL^{-1}, C_0(H_2O_2) = 60 mgL^{-1}, I_L = 16.7 mWcm^{-2}, and a pH of 3.0 at 120 min.

Blank runs performed with 60 mgL^{-1} of AR18 at pH 3.0 for 120 min using magnetite as the catalyst revealed that the Fenton-like process with H_2O_2 and the photolysis UV radiation alone results in less than 10% degradation of the azo dye. Due to the absence of the catalyst, H_2O_2 and UV irradiation offer limitations to the reaction occurrence, where AR18 degradation is meaningless. Even though the photochemical process using UV/H_2O_2 without a catalyst may affect the AR18 degradation with ~80% for 60 mgL^{-1} and ~45% for 200 mgL^{-1} (Figure 1b), the activity is comparatively modest for a heterogeneous photo-Fenton-like process in the presence of magnetite, with a maximum degradation of 95% under the conditions used here.

Based on the abovementioned results, the catalyst dosage is set at 1.4 gL^{-1} in the presence of H_2O_2/UV, which is suitable for undertaking a systematic study of the photodegradation of the AR18 azo dye over Fe_3O_4 as a catalyst. The effects of various Heterogeneous Fenton-like reaction parameters on the degradation efficiency of the AR18 azo dye are evaluated (Figure 2).

The influence of pH for Fenton and Fenton-like reactions, as a parameter to elucidate the availability of Fe^{2+} to decompose H_2O_2 and generate the hydroxyl radicals in Fenton and Fenton-like reactions over iron-based catalysts with pH in the range of 2.5–4.0, is evaluated [20–22].

The degradation efficiencies at the different tested pH levels are related to the zeta potential on the magnetite surface, which was +8.4 mV at pH = 3.0, −6.26 mV at pH = 6.0, and −21.7 mV at pH = 8.0. The AR18 solution at 25 °C has an initial pH of 6 and under this condition, the degradation efficiency is only 7.5% after 30 min of the reaction, while a conversion of 32% can be achieved at pH = 3.0 for the same reaction time. After 60 min, the degradation efficiency improves and activities around 20% are only observed at a natural pH (6.0) and a slightly alkaline pH (8.0). On the contrary, at pH = 3.0, the degradation efficiency increases up to 60.3%. After 120 min, degradation efficiencies were 88% in the acidic medium and approximately 39% and 38% at pHs = 6.0 and 8.0, respectively (Figure 2a). At pH 8.0, the magnetite catalyst is observed to be stable and there is no significant change in the degradation efficiency compared to that observed at an almost neutral pH (pH = 6.0). In general, at pH values close to 3.5, azo dye molecules are effectively

degraded by •OH radicals through the decomposition of H_2O_2 on the catalytic surface of magnetite [11]. Furthermore, the oxidation potential of the •OH/H_2O redox couple is greater at acidic pH values, which favors the degradation efficiency. At higher pH values (alkaline medium), the oxidizing effect decreases due to the reactions between •OH radicals and H_2O_2 [11,23]. Additionally, in an alkaline medium, the photocatalytic treatment of Acid Red 18 on WO_3 microspheres decorated with goethite showed a 16% reduction in degradation when the pH was increased from 1.89 to 9.64. This behavior was attributed to electronic repulsion between the anionic dye molecule and the $^{-}$OH groups attached to the catalyst surface, as can also be seen in this study [24].

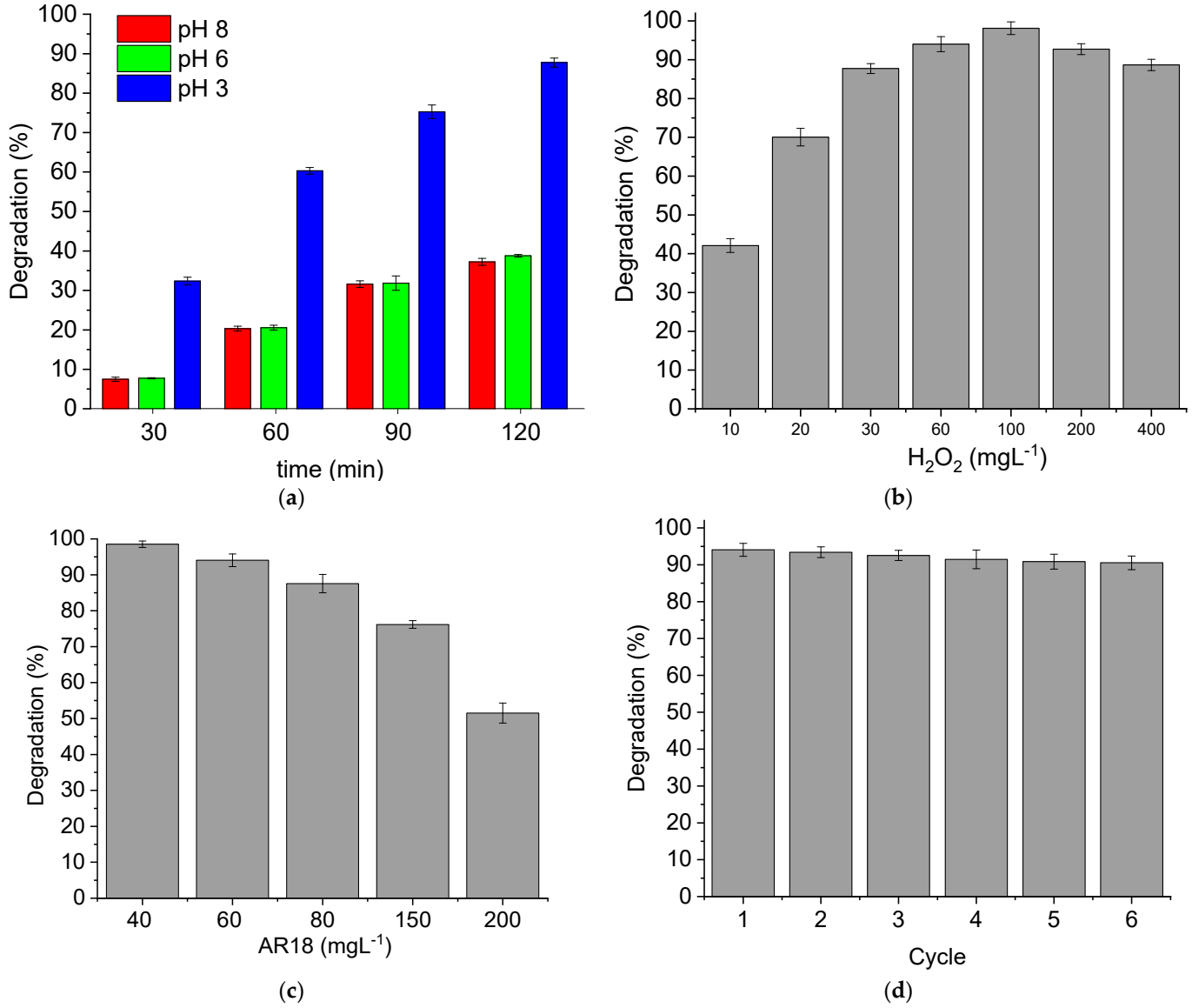

Figure 2. (**a**) Influence of pH with an initial catalyst dosage $C_0(Fe_3O_4)$ of 1.4 gL^{-1} at a fixed condition of C_0(AR18) = 60 mgL^{-1}, $C_0(H_2O_2)$ = 30 mgL^{-1} within 120 min. (**b**) Influence of the initial H_2O_2 concentration using $C_0(Fe_3O_4)$ of 1.4 gL^{-1} and C_0(AR18) of about 60 mgL^{-1} at a pH of 3.0 for 120 min. (**c**) Effect of C_0(AR18) with a $C_0(Fe_3O_4)$ of 1.4 gL^{-1}, $C_0(H_2O_2)$ of 60 mgL^{-1}, and a pH of 3.0 for 120 min. (**d**) Reuse of the Fe_3O_4 at 25 °C after the heterogeneous photo-Fenton reaction using a 1.4 gL^{-1}, C_0(AR18) of 60 mg L^{-1}, $C_0(H_2O_2)$ = 60 mgL^{-1}, I_L = 16.7 mW cm^{-2}, at a pH of 3.0 and t = 120 min.

Because the initial H_2O_2 concertation greatly affects the degradation of AR18 under acidic conditions [22], to understand the heterogeneous photodegradation trend, a wide

range of H_2O_2 concentrations should be considered. Figure 2b illustrates that the degradation of the azo dye increased linearly from 42.1 to 94.1% with a H_2O_2 concentration increment in the range of 10–60 mgL^{-1} within 120 min. With further initial H_2O_2 of up to 100 mgL^{-1}, the degradation efficiency diminished between 2.2% and 9.4%. This might seem counterintuitive because larger amounts of H_2O_2 would likely generate more $^{\bullet}OH$ radicals to degrade the azo dye. However, with an excess of H_2O_2, the rate of $^{\bullet}OH$ recombination increases ($^{\bullet}OH + {}^{\bullet}OH \rightarrow H_2O_2$) and the parallel reaction of $^{\bullet}OH$ consumption by H_2O_2 is favored to form $HO_2^{\bullet}$ or O_2^- ($H_2O_2 + {}^{\bullet}OH \rightarrow H_2O + HO_2^{\bullet}$), which are less reactive species than $^{\bullet}OH$ [25,26].

In addition, it is commonly accepted that the effect of azo dye concentration on Fenton and Fenton-like oxidation is limited at higher concentrations of AR18 due to the effective formation of hydroxyl radicals on the magnetite catalyst [11,22,27]. Accordingly, Figure 2c shows quite an impressive almost complete AR18 degradation efficiency for concentrations below 80 mgL^{-1}. As expected, an azo dye concentration between 150 and 200 mgL^{-1} produces only 76.1% and 51.5%, suggesting that Fe^{2+} species of magnetite can still be present, but its availability might be low, which may be related to the adsorption on the catalyst surface of several intermediate products formed during the oxidative process, including aromatic compounds, naphthalenes, and their hydroxylated and nitrified derivatives, naphtodiols and phthalic acid derivatives [28]. Hence, with the chosen magnetite catalyst loading, 200 mgL^{-1} (0.33 $mmolL^{-1}$) was used for further kinetic and thermodynamics studies of AR18, AR16, and OR2.

The requirement for a stable catalyst in the heterogeneous Fenton-like reaction can be understood based on the recycling experiments. Figure 2d indicates that there are six cycles of consecutive uses of magnetite without any loss of degradation efficiency. At the end of the reaction, a steady state plateau of about 90–94% is reached for the initial AR18 concentration of 60 mgL^{-1}, at a pH of 3.0 for 120 min, with no Fe species leaching as determined by AAS chemical analysis. These results are comparable to those from reports in the literature on spinel isostructural ferrite-based catalysts [11,29,30].

2.2. Kinetics and Thermodynamics of Degradation

According to the findings, reaction kinetics play an important role in determining the rate of heterogeneous photo-Fenton degradation processes [11,29].

The pseudo-first-order model was applied for the AR18, AR66, and OR2 azo des with similar structures. Figure 3 depicts the effect of reaction temperatures in the range of 25–60 °C. At 25 °C, all azo dyes undergo higher degradation efficiency in a shorter reaction time owing to elevated dye concentrations, evidencing a major collision rate between the azo dyes and $^{\bullet}OH$ radicals. With an increase in reaction temperature from 40 to 60 °C, an increment in reaction rate is observable for all azo dyes at short reaction times. As the reaction proceeds, the degradation efficiency reduces, caused by the decreased collision rate between azo dyes, intermediate compounds, and hydroxyl radicals. In agreement, the rate is not affected with respect to the change in temperature within the range of longer reaction times [13,31,32]. The degradation kinetics of azo dyes follow the order: OR2 > AR66 > AR18, with the azo dye OR2 reacting with better efficiency at the three temperatures investigated.

The Arrhenius plots for the photo-Fenton degradation of azo dyes are depicted in Figure 4. The k_1 (min^{-1}) and E_a ($kJmol^{-1}$) parameters are given in Table 1. The Arrhenius plots of the natural logarithm of k_1 are linearly correlated with the reaction temperature, as shown in Figure 4.

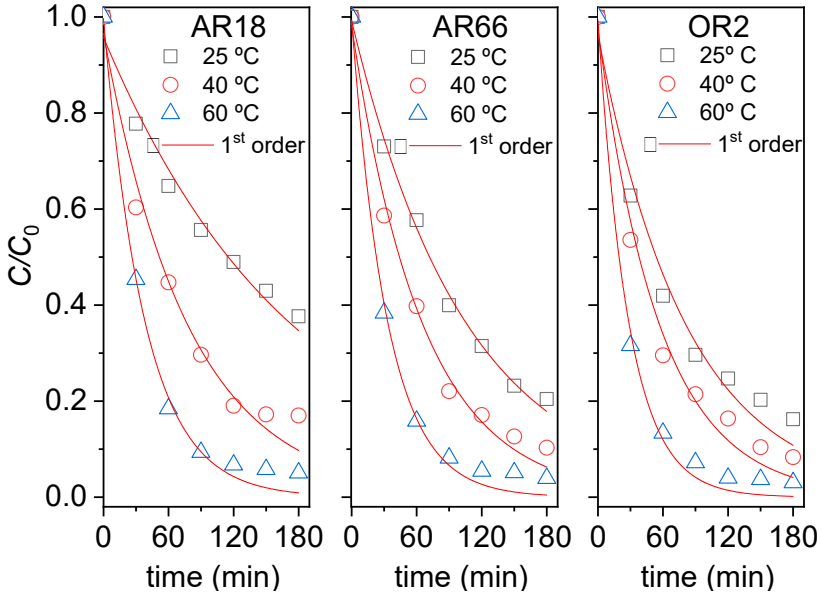

Figure 3. Degradation of AR18, AR66, and OR2 in a heterogeneous photo-Fenton-like process as a function of time. Reaction conditions: $C_0(Fe_3O_4)$ = 1.4 gL^{-1}, C_0(dye) = 0.33 $mmolL^{-1}$, $C_0(H_2O_2)$ = 60 mg L^{-1}, I_L = 16.7 $mWcm^{-2}$, and a pH of ca. 3.0.

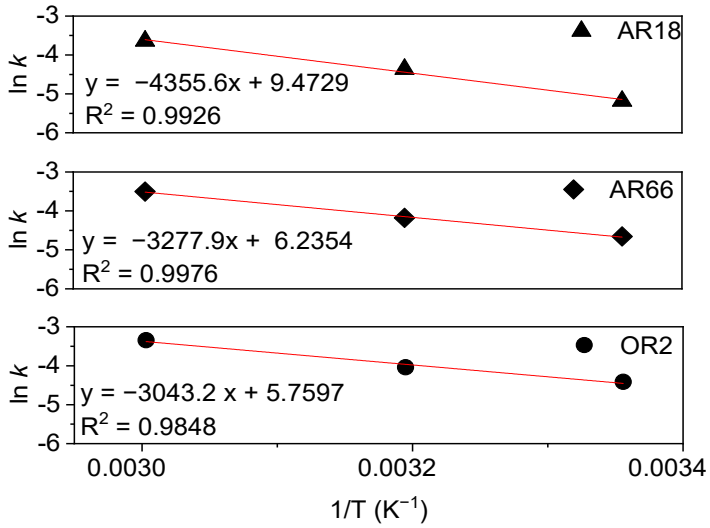

Figure 4. Arrhenius plots for heterogeneous photo-Fenton degradation of AR18, AR66, and OR2. $C_0(Fe_3O_4)$ = 1.4 gL^{-1}, C_0(dye) = 0.33 $mmolL^{-1}$, $C_0(H_2O_2)$ = 60 mgL^{-1}, I_L = 16.7 $mWcm^{-2}$, and a pH of ca. 3.0.

Table 1. Pseudo-first-order rate constant and activation energy for AR18, AR66, and OR2 degradation via the heterogeneous photo-Fenton process. $C_0(Fe_3O_4)$ = 1.4 gL^{-1}, C_0(dye) = 0.33 $mmolL^{-1}$, $C_0(H_2O_2)$ = 60 mgL^{-1}, I_L = 16.7 $mWcm^{-2}$, and a pH of ca. 3.0.

T (°C)	AR18			AR66			OR2		
	k_1 (min^{-1})	R^2	E_a ($kJmol^{-1}$)	k_1 (min^{-1})	R^2	E_a ($kJmol^{-1}$)	k_1 (min^{-1})	R^2	E_a ($kJmol^{-1}$)
25	0.0056	0.980		0.0095	0.997		0.0122	0.979	
40	0.0127	0.981	36.2	0.0153	0.992	27.2	0.0176	0.986	25.3
60	0.0262	0.994		0.0301	0.994		0.0353	0.994	

Photodegradation of the azo dyes on the magnetite surface is relied upon to improve the degradation efficiency. The examined kinetic data show a high correlation coefficient of 0.97 with a good fitting between calculated and experimental values, suggesting that the heterogeneous Fenton-like process follows first-order kinetics (Table 1). In addition, the reaction rates of color removal and degradation efficiencies increase with increasing temperature, with the heterogeneous photo-Fenton oxidation reaction being suitable. In fact, the activation energy of AR18 is 36.2 kJmol^{-1}, comparable with the degradation efficiency of Fe-based catalysts on the Acid Red 18 azo dye in other studies [21,29,31–34]. For OR2, the calculated activation energy is 25.3 kJmol^{-1}, comparable with reports in the literature on magnetite-based catalysts [35–38]. The large amount of surface Fe^{2+}/Fe^{3+} sites in the magnetite catalyst may influence the kinetics of the heterogeneous photodegradation Fenton reaction.

The parameter determination of Gibbs (ΔG), entropy (ΔS), and enthalpy (ΔH) for the photodegradation of AR18, AR66, and OR2 is based on the van't Hoff equation in Figure 5. The obtained data are summarized in Table 2.

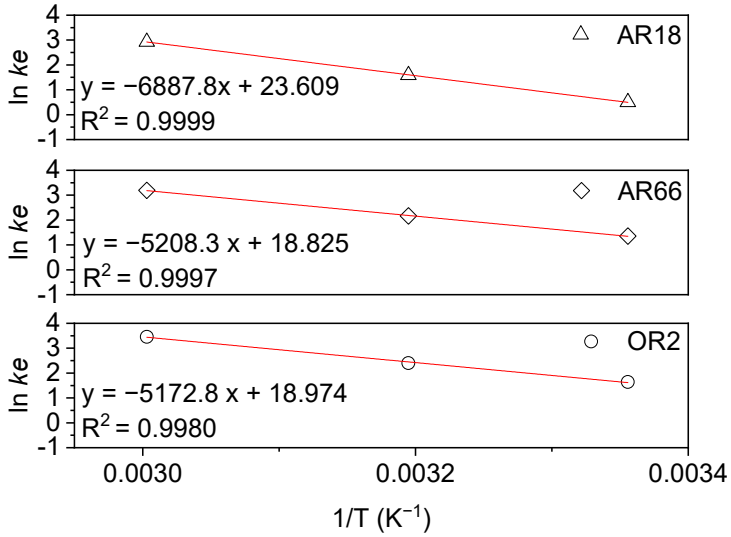

Figure 5. The van't Hoff plots for the heterogeneous photo-Fenton degradation of AR18, AR66, and OR2. $C_0(Fe_3O_4)$ = 1.4 gL^{-1}, C_0(dye) = 0.33 mmolL^{-1}, $C_0(H_2O_2)$ = 60 mgL^{-1}, I_L = 16.7 mWcm^{-2}, and a pH of ca. 3.0.

Table 2. Thermodynamic parameters for AR18, AR66, and OR2 azo dye degraded using the heterogeneous photo-Fenton. $C_0(Fe_3O_4)$ = 1.4 gL^{-1}, C_0(dye) = 0.33 mmolL^{-1}, $C_0(H_2O_2)$ = 60 mgL^{-1}, I_L = 16.7, and mWcm^{-2} at a pH of 3.0.

T (°C)	ΔH (kJmol^{-1})	ΔS (kJmol^{-1}K^{-1})	ΔG (kJmol^{-1})
		AR18	
25			−1.25
40	57.3	0.196	−4.13
60			−8.12
		AR66	
25			−3.37
40	43.3	0.157	−5.64
60			−8.84
		OR2	
25			−4.07
40	43.1	0.158	−6.25
60			−9.58

The enthalpy (ΔH) values obtained for the AR18, AR66, and OR2 azo dyes are all similar to those of [39], which analyzed Acid Red 27. The ΔS values for AR18, AR66, and OR2 are 0.196, 0.157, and 0.158 kJmol^{-1}K^{-1}, respectively, suggesting that the reaction is more spontaneous with increasing temperatures [40]. The ΔG values for the OR2 degradation in the range of temperatures investigated are higher than those found for AR66 and AR18, which corroborates with the degradation order and the reaction kinetics (OR2 > AR66 > AR18).

This behavior can be explained in terms of molecular effects related to the polar group natures, possible steric hindrance, and, to some extent, the type of aromatic ring conjugation in the azo dye structure. OR2 and AR18 are hydroxyl azo aqueous species forming hydrazones (*o*-ortho and/or *p*-para), while AR 66 is typically an amino azo dye where azo tautomeric arrangements predominate [41], despite the formation of the *o*-hydrazone in another molecular region.

Particularly, the OR2 azo dye occurs as an *o*-hydrazone (Figure 6a) without perturbation of the sulphonate group (–SO_3^-), which is *p*-substituted in the phenyl (ph), while in AR18 (Figure 6b), the *o*-hydrazone is protected or hindered by –SO_3^- at positions 2 and 4 of the naphtyl (naph) group adjacent to the azo bond, and there is a third –SO_3^- *p*-substituted group in the second naphtyl group of the molecule. Thus, the high number of sulphonate groups in AR18 inhibits the attack of $^{\bullet}$OH and other reactive oxygen species (ROS) by electrostatic repulsion, increasing steric hindrance and reducing the accessibility of oxidizing radicals ($^{\bullet}$OH, $O_2^{\bullet -}$, $HO_2^{\bullet}$) to azo groups and aromatic azo rings [42]. Under these conditions, OR2 is easily degraded by ROS generated on the Fe_3O_4 (≡Fe^{3+}) surface catalyst of AR18, as observed in the direct photodegradation of these dyes by UV irradiation in a rotating disk photoreactor [43]. In this direct photolysis, the pseudo-first-order constant ratio for Orange 2 and Acid Red 18 (k_1 OR2/k_1 AR18) was 1.97, which is similar (~2.17) to that found in a work on heterogeneous photodegradation using synthesized magnetite. For AR66, the k_1 (min^{-1}) is between the k_1 for OR2 and AR18, which can be explained by the function of minor steric hindrance and electrostatic repulsion generated from two structural sulphonates situated in position 2 of the *o*-hydrazone and another *p*-substituted in the phenyl group associated with the second azo group of the molecule (Figure 6c). In addition, the conjugation of the rings increments in the disulphonate (AR66) type: naph-azo-ph-azo-ph is more favorable to photoconversions than the naph-azo-naph conjugation present in AR18 (trisulphonate).

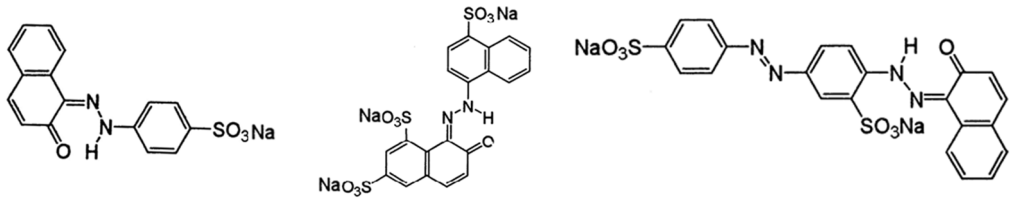

(**a**) (**b**) (**c**)

Figure 6. Azo dye structures in a study adapted from worlddyevariety.com (accessed on 28 August 2024). (**a**) OR2. (**b**) AR18. (**c**) AR66.

Based on the hard/soft acid/base (HSAB) of Pearson theory [44], Fe^{3+} is typically a strong Lewis acid (HA) with a high affinity for strong Lewis (HB), providing ionic interactions for base HA/HB complex interactions. On the other hand, azo dyes can be characterized as soft bases (SB) with a basic character that decreases with increasing carbonic chain length, generating a diffuse electron distribution. Therefore, the minor molecular complexities (MC) and topological polar surface area (PSA) in OR2 (MC = 529, PSA = 111 Å) and AR18 (MC = 958, PSA = 201 Å) in comparison with AR18 (MC = 1080, PSA = 242 Å) (data obtained from Pubchem databases) can favor catalytic surface interactions, promoting heterogeneous mechanistic oxidation. In this order, the polar covalent interaction features

in the conjugated Fe^{3+}//OR2 complex are stronger than in the Fe^{3+}//AR18 base system, whereas the Fe^{3+}//AR66 conjugated par appears as an intermediate character.

When considering catalyst participation in the processes, it is important to figure out the position and nature of the two active iron species on the surface ($\equiv Fe^{3+}$ and/or $\equiv Fe^{2+}$) in contact with the reactive functional groups (–N=N–, $–SO_3^-$, –C=C–) of the excited dye molecule (dye*). The heterogeneous photo-Fenton process is described by the following equations (Equations (1)–(6)), with $^{\bullet}OH$ generation due to the direct photolysis of H_2O_2 at 180–340 nm (photochemistry reaction, Equation (2)), along with iron cations (photocatalytic reactions, Equations (3) and (4)) [3,15,45].

$$dye + h\lambda \rightarrow dye^* \quad (1)$$

$$H_2O_2 + h\lambda \rightarrow 2\,{}^{\bullet}OH \quad (2)$$

$$\equiv Fe^{3+} + H_2O_2 + h\lambda \rightarrow \equiv Fe^{2+} + {}^{\bullet}OH + H^+ \quad (3)$$

$$\equiv Fe^{2+} + H_2O_2 \rightarrow \equiv Fe^{3+} + {}^{\bullet}OH + {}^{-}OH \quad (4)$$

$$\equiv Fe^{2+} + H_2O_2 \rightarrow \equiv Fe^{3+} - OH + {}^{-}OH \quad (5)$$

$$dye^* \text{ (organic)} + {}^{\bullet}OH \rightarrow \text{products} \quad (6)$$

Synthesized magnetite is a magnetic mixture of hematite (α-Fe_2O_3), maghemite (γ-Fe_2O_3), and goethite (α-FeOOH), with about 70% of Fe_3O_4 and 30% of the aforementioned phases [46]. Such a composition is non-stoichiometric and is abundant in iron species that act favorably in the formation of $^{\bullet}OH$ radicals. Figure 7 shows a comparison of the degradation of AR18 using various iron oxides with different Fe^{3+}/Fe^{2+} molar ratios, for instance, the wüstite (FeO, $Fe^{3+}/Fe^{2+} = 0$), goethite (FeOOH, $Fe^{3+}/Fe^{2+} = \infty$), hematite (Fe_2O_3, $Fe^{3+}/Fe^{2+} = \infty$), and magnetite (Fe_3O_4, $Fe^{3+}/Fe^{2+} = 2$) prepared in this study.

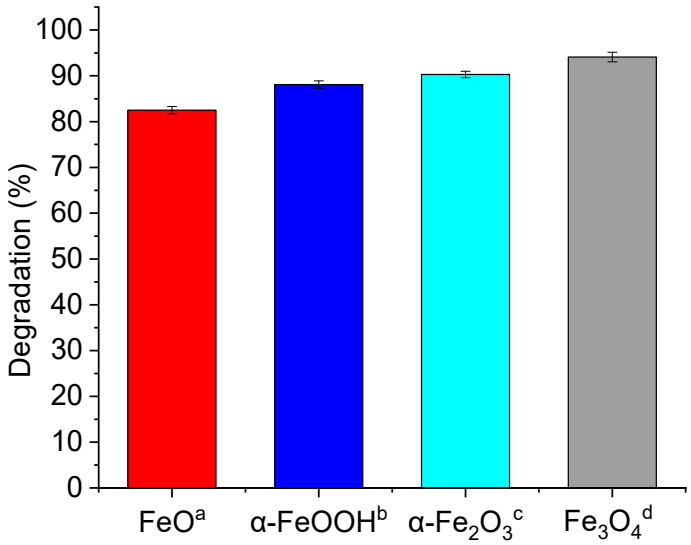

Figure 7. Comparison of the degradation efficiency of the AR18 azo dye at 25 °C over distinct iron catalysts via the heterogeneous photo-Fenton process. Catalyst dosage = 1.4 gL^{-1}, C_0(AR18) = 60 mgL^{-1}, $C_0(H_2O_2)$ = 60 mgL^{-1}, I_L = 16.7 $mWcm^{-2}$, and a pH of 3.0 at 180 min. [a] Synthesized according to [47], [b] Synthesized according to [48], [c] Commercial (Sigma-Aldrich, St. Louis, MO, USA), and [d] synthesized in this work.

At 25 °C, the initial concentration of 60 mgL^{-1} of the dye is not a limiting factor for the catalytic activity of the various iron oxides (Figure 7), as observed, for example, at the concentration of 200 mgL^{-1} of Acid Red 18, where the maximum degradation was 62.3% (Figure 1b). The similar degradations indicate similar mechanistic considerations for the catalytic surface. Despite the oxy (hydroxide) nature of goethite, the major Fe^{3+} proportion

seems to contribute to slightly higher oxidation than FeO, possessing only Fe^{2+} sites. In photo-Fenton systems with high Fe^{2+} concentrations under acidic conditions, Fe^{2+} exists in the $Fe(OH)^{2+}$ form, which determines a lower •OH radical generation and a decrease in the degradation rate [49,50].

Comparisons of the use of AR66, OR2, and AR18 dyes using iron oxide-based catalysts in Heterogeneous Fenton processes are given in Table 3.

Table 3. Comparison of the catalytic performance of iron oxide-based catalysts in the heterogeneous Fenton process over AR66, OR2, and AR18 dyes.

Dye	Process	Degradation Rate	Reference
AR66	Homogeneous Fenton: pH = 3.5, 45 °C, 180 min, C_0(dye) = 16.4 mgL^{-1}, $C_0(Fe^{2+})$ = 6.95 mgL^{-1}, $C_0(H_2O_2)$ = 25.5 mgL^{-1}	99.6%	[12]
AR18	Electro-Fenton: pH = 3.0, 5 min, C_0(dye) = 100 mgL^{-1}, $C_0(H_2O_2)$ = 400 mgL^{-1}, catalyst: iron plane electrodes (80 cm^2), voltage = 30 V, C_0(NaCl) = 100 mgL^{-1}	99.9%	[22]
AR18	Heterogeneous photo-Fenton with ultrasonic irradiation: pH = 3.0, 25 °C, 5 min, lamp. = Visible (495 W), C_0(dye) = 60 mgL^{-1}, $C_0(WO_3$-FeOOH) = 0.67 gL^{-1}, $C_0(H_2O_2)$ = 1000 mgL^{-1}	~92.6%	[24]
AR18	Heterogeneous Fenton: pH = 3.0, 25 °C, 60 min, C_0(dye) = 500 mgL^{-1}, $C_0(Fe^0)$ = 80 mgL^{-1}, $C_0(H_2O_2)$ = 500 mgL^{-1}	~81.2%	[27]
AR18	Photocatalytic: pH = 3.0, 50 min, lamp. = 2 UVC, C_0(dye) = 10 mgL^{-1}, $C_0(AgCoFe_2O_4$@Ch/AC) = 0.14 gL^{-1}	~96.7%	[29]
OR2	Heterogeneous Fenton: pH = 3.0, 25 °C, 180 min, C_0(dye) = 70 mgL^{-1}, C_0(V-Ti-Fe_3O_4) = 1.0 gL^{-1}, $C_0(H_2O_2)$ = 340 mgL^{-1}	98%	[35]
OR2	Heterogeneous photo-Fenton: pH = 3.0, 30 °C, 20 min, lamp: UVC (6 W), C_0(dye) = 70 mgL^{-1}, $C_0(Fe_3O_4$@γ-$Fe_2O_3)$ = 1 gL^{-1}, $C_0(H_2O_2)$ = 340 mgL^{-1}, C_0(oxalate) = 44 mgL^{-1}	100%	[45]
OR2	Heterogeneous Fenton: pH = 2.7, 30 min, 42 °C, C_0(dye) = 100 mgL^{-1}, $C_0(Fe_3O_4)$ = 1.5 gL^{-1}, $C_0(H_2O_2)$ = 748 mgL^{-1}	~99.5%	[50]
AR18	Heterogeneous photocatalytic ozonation: Air/O_3 = 200 mgh^{-1}, pH = 3.0, 60 min, lamp. = UVA-UVB (35.4 Wm^{-2}), C_0(dye) = 50 mgL^{-1}, $C_0(Fe_3O_4)$ = 0.5 gL^{-1}, $C_0(H_2O_2)$ = 1122 mgL^{-1}	99%	[51]
AR18	Heterogeneous photo-Fenton: pH = 3.0, 25 °C, 120 min, lamp. = UVC (7 W), C_0(dye) = 60 mgL^{-1}, $C_0(Fe_3O_4)$ = 1.4 gL^{-1}, $C_0(H_2O_2)$ = 60 mgL^{-1}	95%	This study
AR18, AR66, OR2	Heterogeneous photo-Fenton: pH = 3.0, 60 °C, 180 min, lamp. = UVC (7 W, 16.7 $mWcm^{-2}$), C_0(dye) = 0.33 $mmolL^{-1}$, $C_0(Fe_3O_4)$ = 1.4 gL^{-1}, $C_0(H_2O_2)$ = 60 mgL^{-1}	94.9%, 96.1%, 97.1%	This study

Although all iron oxide-based catalysts evaluated in heterogeneous Fenton processes have good efficiencies, the present study shows low leaching of the active Fe sites of magnetite, with a degradation efficiency comparable with those reported in the literature [12,22,45]. Among the three dyes, AR18 is more reactive than OR2 and AR66 and, over magnetite, shows an easier separation of the solution and great potential applications for photocatalysis.

2.3. Treated Solution Characterization

Figure 8 shows the UV–Vis spectra of the OR2 azo dye treatment after the heterogeneous photo-Fenton reaction over the synthesized Fe_3O_4. The structural iron reacts with H_2O_2, giving rise to •OH radicals, which attack the azo (–N=N–) groups, producing

effective solution decolorization in 90 min of photodegradation. The UV decolorization at 230 nm and 310 nm is related to the benzene, the naphthalene ring, as shown in reports in the literature, although these bands have a much lower and slower intensity than the chromophore band positioned at 485 nm. These behaviors are similar to those observed in the degradation of the azo dyes Reactive Black 5 and Orange 2 [50,52], indicating a high decolorization of the OR2 accompanied by a relative concentration of the residual compounds after the oxidative reactions. Regarding the chemical oxygen demand (COD) before and after the heterogeneous photo-Fenton reaction, only a 29.7% reduction in the chemical oxidation of organic matter was observed, which is similar to the 27% COD reduction reported in the degradation of Acid Red 73 dye by the heterogeneous photo-Fenton process [53]. These results reveal the need for long reaction times or harsh treatment conditions, aiming for mineralization of the refractory compounds produced.

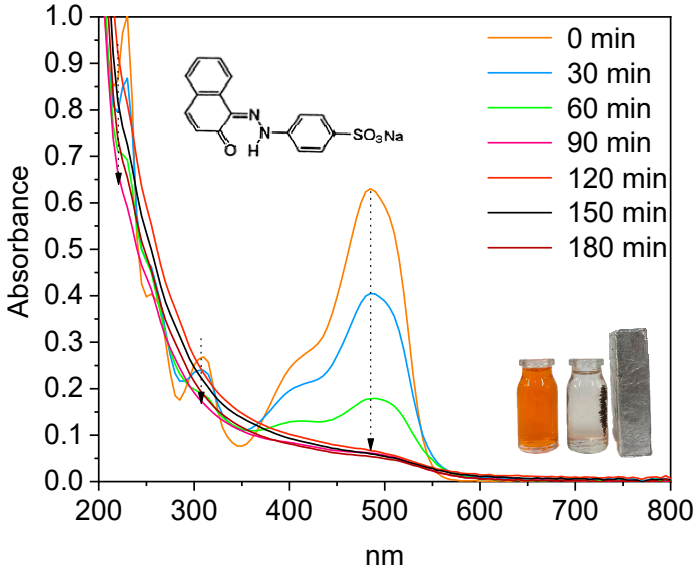

Figure 8. UV–Vis spectra of Orange 2 as a function of reaction time at 60 °C in the heterogeneous photo-Fenton-like reaction. Catalyst dosage = 1.4 gL^{-1}, C_0(dye) = 0.33 $mmolL^{-1}$, $C_0(H_2O_2)$ = 60 mgL^{-1}, and I_L = 16.7 $mWcm^{-2}$ at a pH of 3.0.

2.4. Spent Magnetite Characterization

The fresh magnetite characterizations are given in our previous reports [46]. XPS spectra of fresh and spent magnetite after the heterogeneous photo-Fenton-like reaction are shown in Figure 9. The XPS spectrum of fresh Fe_3O_4 (Figure 9a) is depicted with the main spin-orbit split peaks located at 710.2 and 724.9 eV (Table 4) for the doublet Fe $2p_{3/2}$–Fe $2p_{1/2}$, respectively. These doublet peaks arise along with their shake-up satellites, typically confirming that the magnetite has Fe species in both divalent Fe^{3+} and Fe^{2+} states [54]. Accordingly, the peak at about 710.8 eV is assigned to the Fe^{3+} ions in octahedral sites, whereas the one located at 723.9 eV indicates the presence of the Fe^{2+} species [55].

The recorded O 1*s* core level has three different oxygen species. A major contribution at 529.6 eV corresponds to 63% due to the existence of lattice oxygens from the Fe-O bonds in Fe_3O_4, as previously detected in the literature [56]. This contribution is accompanied by two other weak components near 531.0 eV (29%), from the OH groups of physisorbed water molecules, and 532.7 eV (8.0%), agreeing well with carbon bonded to oxygen species, e.g., –C–O– and –C=O [46,56].

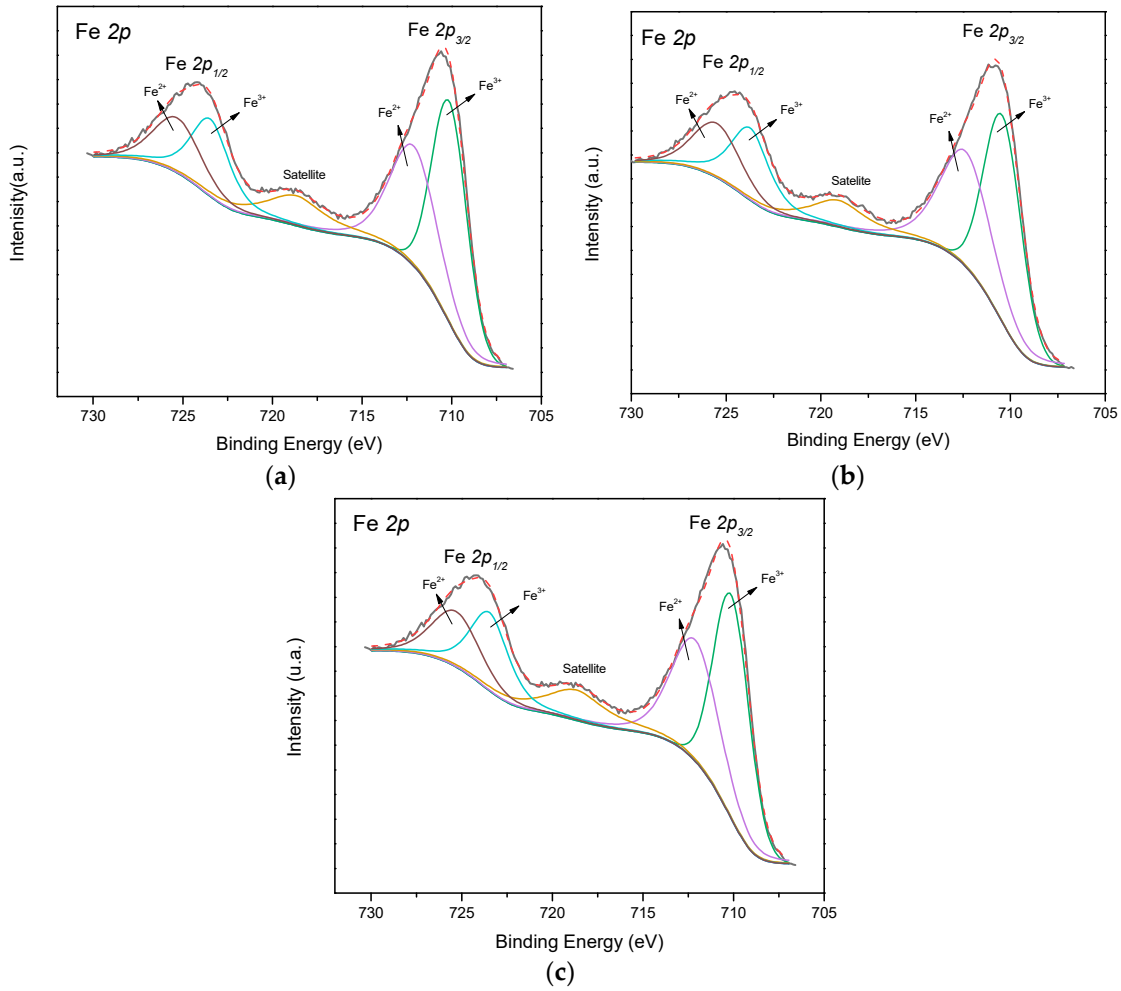

Figure 9. XPS spectra of Fe 2*p* core levels for magnetite. (**a**) Fresh Fe_3O_4, and after the heterogeneous photo-Fenton-like process with (**b**) AR18 and (**c**) AR 66. Reaction conditions: Catalyst dosage = 1.4 gL^{-1}, C_0(dye) = 0.33 $mmolL^{-1}$, $C_0(H_2O_2)$ = 60 mgL^{-1}, and I_L = 16.7 $mWcm^{-2}$ at a pH of 3.0 at 60 °C.

Table 4. XPS parameters of the fresh and spent magnetite after reaction with AR18 and AR66 dyes. Reaction conditions: Catalyst dosage = 1.4 gL^{-1}, C_0(dye) = 0.33 $mmolL^{-1}$, $C_0(H_2O_2)$ = 60 mgL^{-1}, and I_L = 16.7 $mWcm^{-2}$ at a pH of 3.0 at 60 °C.

Sample	Binding Energy (eV)					
	Fe $2p_{3/2}$	Fe $2p_{1/2}$	C 1*s*	O 1*s*	S $2p_{3/2}$	Fe^{3+}/Fe^{2+} Ratio
Fe_3O_4	710.0 (18)	724.9 (17)	284.7 (82) 286.0 (12) 288.3 (6)	529.6 (63) 531.0 (29) 532.7 (8)		2.3 [46]
Fe_3O_4/AR18	710.3 (17)	724.8 (23)	284.8 (80) 285.3 (12) 288.5 (8)	529.9 (63) 531.4 (28) 532.7 (9)		2.6
Fe_3O_4/AR66	710.2 (19)	724.7 (21)	284.8 (81) 285.3 (13) 288.6 (6)	529.8 (56) 531.4 (28) 532.8 (16)	168.1	2.4

Moreover, the Fe^{3+}/Fe^{2+} atomic composition obtained from the area ratio between the peak at 711.2 and 710 eV is 2.3 (Table 4), suggesting that there is a distribution of Fe^{3+} and Fe^{2+} ions between the different sites of magnetite, which has a highly oxidized surface [46].

The C 1*s* core level appears with binding energies ascribed to –C=C– and adventitious carbon as the dominant peak at 284.7 eV (82%), along with peaks of –C–OH at 286.0 eV (12%) and –C–C=O at 288.3 eV (6%), in agreement with the findings [54–57].

To further verify the surface stability of the magnetite, the AR18 and AR66 azo dyes are degraded using the heterogeneous photo-Fenton-like reaction. Table 4 summarizes the binding energies of the magnetite after the catalytic reaction with the dyes. The XPS spectra of the magnetite after the heterogeneous photo-Fenton-like reaction with AR18 and AR66 (Figure 9b,c) show similar results, indicating that the valence states of iron are not changed after the title reaction. Similarly, after dye degradation, C 1*s* and O 1*s* core levels have comparable values with those of the fresh magnetite (Table 4). Moreover, the expected N 1*s* core level for Fe_3O_4/AR18 and Fe_3O_4/AR66, with a binding energy close to 400 eV, is not found after the reaction [46]. It could be associated with the weak chemisorption of the nitrogen groups of the dye on the sample.

In particular, the S 2*p* core level appears only for Fe_3O_4/AR66, having binding energy at 168.1 eV due to S-O groups [46]. Additionally, the detected sulfate species on the surface of magnetite after the AR66 Fenton-like reaction would contribute to the physisorption of the Fe active sites on magnetite, providing a low performance of the solid using the AR66 dye.

The atomic concentration percentages of Fe, C, and O in fresh Fe_3O_4 are 29.3, 56.5, and 14.4%. Comparison with the atomic concentrations of the components of the two dyes shows values of C: 41.5%, O: 45.7%, and Fe: 12.6% and C: 37.5%, O: 51.6%, Fe: 10.8%, and S: 0.18% for Fe_3O_4/AR18 and Fe_3O_4/AR66, with deviations within the limits of precision and accuracy for the XPS technique.

In addition, Table 4 indicates that the Fe^{3+}/Fe^{2+} atomic ratio involves a 2.4–2.6 range for both dyes, which might be expected according to the surface composition of magnetite [58]. It suggests magnetite's stability towards the reaction, due to the low leaching of the iron species in the solution, after the reaction. Importantly, the magnetite has low activity in the photodegradation of the dyes by the heterogeneous Fenton-like degradation reaction compared with TiO_2, cobaltite, and other catalysts [59–61].

3. Materials and Methods

3.1. Materials

Pure Acid Red 18 ($C_{20}H_{11}N_2Na_3O_{10}S_3$, 604.48 $gmol^{-1}$) azo dye was purchased from Acros Organics (Fair Lawn, NJ, USA). Orange 2 ($C_{16}H_{11}N_2NaO_4S$, 85%, 350.32 $gmol^{-1}$) and Acid Red 66 ($C_{22}H_{14}N_4Na_2O_7S_2$, 55%, 566.48 $gmol^{-1}$) azo dyes were obtained from Sigma-Aldrich (St. Louis, MO, USA). All azo dye reagents were used without further purification. The hydrogen peroxide solution (H_2O_2, 30 wt. %) was purchased from Êxodo Científica (Êxodo Científica, São Paulo, Brazil). Prior to the use, the content of H_2O_2 was evaluated using the permanganate method [62]. Sulfuric acid (H_2SO_4, 98%) was obtained from Vetec (Vetec, Rio de Janeiro, Brazil). Deionized water was used in all experiments.

3.2. Catalyst Synthesis and Characterizations

Fe_3O_4 consisting primarily of surface Fe^{3+} and Fe^{2+} ions was synthesized by a coprecipitation method, as found elsewhere [46,63]. The physicochemical characterizations of the magnetite in this study are given in ref. [46]. The zeta potential and the particle size distributions at pH of 3.0, 6.0, and 8.0 were performed in a Zetasizer Nano S apparatus from Malvern (GBR, Cambridge, UK)). The surface compositions and valence state of the elements present in the spent samples used at distinct reaction conditions were determined by X-ray photoelectron spectroscopy (XPS). XPS spectra were obtained on a PHI VersaProbe II Scanning XPS Microprobe from Physical Electronics (Minneapolis, MN, USA). The incident radiation was generated by the Al Kα X-ray source, operating at 1486.6 eV and 15 kV. The spectra were calibrated using the binding energy peak of C 1*s* at 284.8 eV from adventitious carbon.

3.3. Heterogeneous Photo-Fenton-Like Oxidation

The heterogeneous photodegradation activity of the magnetite was conducted in a borosilicate reactor (height of ca. 13 cm; diameter of 6.5 cm) with a capacity of about 45 mL coupled to a circulating water jacket to maintain solution temperature. A UV-C Philips TUV PL-S 7W/2P model lamp of ca. 7.1 W was positioned to the reaction reactor (Philips, Pila, PL, Poland). The lamp generated UV irradiation at 254 nm with a radiation intensity (I_L) of ca. 16.7 mWcm^{-2}.

Typically, for heterogeneous photo-Fenton-like batch experiments, the reaction was initiated by introducing the H_2O_2 solution along with the azo dyes to the reaction system. Then, air flow at a 180 ± 20 mLmin^{-1} rate was introduced into the system, which was used to produce a homogeneous solution. The abovementioned suspension was exposed to the UVC lamp under constant irradiation (16.7 mWcm^{-2}) and aliquots were withdrawn to determine the concentration of the azo dye solutions using a UV–Vis spectrophotometer.

The effects of the initial concentration of azo dye, the initial concentration of H_2O_2, catalyst dosage, and pH were evaluated for AR18 at 25 °C, while the kinetic and thermodynamic parameters were evaluated at 25, 40, and 60 °C for the three azo dyes (AR18, AR66, and OR2) under constant radiation of 16.7 mWcm^{-2}, an initial dye concentration of 0.33 mmolL^{-1}, and at ideal values of catalyst dosage, pH, and H_2O_2 concentration. The molar concentration (0.33 mmolL^{-1}) was chosen to guarantee an identical quantity of dye molecules in the reaction with the catalyst and peroxide under the same pH and irradiation conditions.

In addition, the initial dosage of the catalyst was taken from reports in the literature [50]. Iron concentrations in solution were estimated by atomic absorption spectrophotometry using Thermo Scientific AAS iCE 3000 equipment (Thermo Fisher Scientific, Waltham, MA, USA). All experiments were performed in duplicate.

The heterogeneous photo-Fenton-like degradation percentage was calculated as follows (Equation (7)). Dye degradation was estimated based on the reduction in absorbance related to the azo group in each dye, which was associated with a calibration curve constructed for each molecule. The calibration curve of each azo dye was set at 505, 510, and 485 nm for AR18, AR66, and OR2, respectively, using a Thermo Fisher UV–Vis Genesys 60 S spectrophotometer (Waltham, MA, USA).

$$\%\text{Degradation} = \left(\frac{C_0 - C_t}{C_0}\right) \times 100 \quad (7)$$

where: C_0 (mmolL^{-1}) and C_t (mmolL^{-1}) are the initial and final azo dye concentrations at a given period, respectively.

To understand the degradation kinetics of the azo dyes at 25, 40, and 60 °C, the pseudo-first-order kinetic model was used, according to Equation (8) [34]:

$$C = C_0 e^{-k_1 t} \quad (8)$$

where: C_0 is the initial concentration of dye (mmolL^{-1}), C is the dye concentration (mmolL^{-1}) at a certain reaction time t (min), and k_1 (min^{-1}) is the rate constant for the pseudo-first-order reaction.

The activation energy (E_a, kJmol^{-1}) of the studied AR18, AR66, and OR2 azo dyes was determined by the Arrhenius equation (Equation (9)), as reported in a previous study [40]:

$$k_1 = A\mathrm{e}^{\frac{-E_a}{RT}} \quad (9)$$

where: A is the Arrhenius constant, k_1 is the rate constant for the pseudo-first-order reaction, T is the absolute (K), and R is the universal constant of the gases (8.314 Jmol^{-1}K^{-1}).

The variations of free Gibbs energy (ΔG), entropy (ΔS), and enthalpy (ΔH) were determined according to the van't Hoff equations [64].

$$k_e = \frac{C_{A_e}}{C_{S_e}} \tag{10}$$

$$\Delta G^\circ = -RT \ln k_e \tag{11}$$

$$\ln k_e = \frac{\Delta S^\circ}{R} - \frac{\Delta H^\circ}{RT} \tag{12}$$

where: k_e is the equilibrium constant and C_{A_e} and C_{S_e} are the degraded and remaining azo dye concentrations in the equilibrium, respectively.

4. Conclusions

At 25 °C, the synthesized magnetite showed photodegradation efficiency of 62.3% for AR18, 79.6% for AR66, and 83.8% for OR2 azo dyes under usual conditions of 1.4 gL^{-1} of catalyst, 60 mgL^{-1} of H_2O_2, pH = 3.0, and constant irradiation of 16.7 $mWcm^{-2}$. Under these conditions, the degradation of the dyes was more than 94% at 60 °C for AR18. The material showed similar catalytic activity after six consecutive reaction cycles, confirming its resistance against leaching of the active sites, as evidenced by XPS and AAS spectroscopy. The kinetics were typically first-order while the thermodynamic studies confirmed the endothermic and spontaneous degradation processes, with reactivity in the following order: OR2 > AR66 > AR18. The activation energy and enthalpy values found for AR18 were 10 and 14 $kJmol^{-1}$, respectively. Moreover, the OR2 molecule was the most easily degraded due to its lower structural complexity, lower steric hindrances, and lower electrostatic repulsion with reactive oxygen species on the catalyst surface. This study showed the promising nature of photo-Fenton technology using magnetite as a catalyst in the treatment of aqueous solutions contaminated with azo dyes, also allowing us to discuss and explain the effect of some chemical characteristics of the target molecule on the performance of oxidative degradation.

Author Contributions: Conceptualization, formal analysis, R.S.A.; methodology, J.A.S.R. and J.F.A.; investigation, R.S.A.; methodology, B.C.B.S.; writing—original draft preparation, writing—review and editing, funding acquisition, A.C.O., R.S.A. and E.R.-C. All authors have read and agreed to the published version of the manuscript.

Funding: The authors acknowledge the financial support from the Ministerio de Ciencia e Innovación, Spain (Grant TED2021-130756B-C31 MCIN/AEI/10.13039/501100011033) and ERDF A way of making Europe by the European Union NextGenerationEU/PRTR.

Data Availability Statement: The data presented in this study are available upon request from the corresponding authors.

Acknowledgments: J.A.S.R. acknowledges the financial support for his master scholarship from the Conselho Nacional de Desenvolvimento Científico Tecnologico (CNPq), Brazil.

Conflicts of Interest: The authors declare no conflicts of interest.

References

1. Chen, Z.; Yan, Y.; Lu, C.; Lin, X.; Fu, Z.; Shi, W.; Guo, F. Photocatalytic self-Fenton system of g-C_3N_4-based for degradation of emerging contaminants: A review of advances and prospects. *Molecules* **2023**, *28*, 5916. [CrossRef]
2. Zhang, Z.; Bai, Z.; Yu, S.; Meng, X.; Xiao, S. Photo-Fenton efficient degradation of organic pollutants over S-scheme ZnO@NH_2-MIL-88B heterojunction established for electron transfer channel. *Chem. Eng. Sci.* **2024**, *288*, 119789. [CrossRef]
3. Magomedova, A.; Isaev, A.; Orudzhev, F.; Sobola, D.; Murtazali, R.; Rabadanova, A.; Shabanov, N.S.; Zhu, M.; Emirov, R.; Gadzhimagomedov, S.; et al. Magnetically separable mixed-phase α/γ-Fe_2O_3 catalyst for photo-Fenton-like oxidation of Rhodamine B. *Catalysts* **2023**, *13*, 872. [CrossRef]
4. Nchimi Nono, K.; Vahl, A.; Terraschke, H. Towards high-performance photo-Fenton degradation of organic pollutants with magnetite-silver composites: Synthesis, catalytic reactions and in situ insights. *Nanomaterials* **2024**, *14*, 849. [CrossRef] [PubMed]

5. Feijoo, S.; González-Rodríguez, J.; Fernández, L.; Vázquez-Vázquez, C.; Feijoo, G.; Moreira, M.T. Fenton and photo-Fenton nanocatalysts revisited from the perspective of life cycle assessment. *Catalysts* **2020**, *10*, 23. [CrossRef]
6. Ismail, G.A.; Sakai, H. Review on effect of different type of dyes on advanced oxidation processes (AOPs) for textile color removal. *Chemosphere* **2022**, *291*, 132906. [CrossRef] [PubMed]
7. Dong, C.; Fang, W.; Yi, Q.; Zhang, J. A comprehensive review on reactive oxygen species (ROS) in advanced oxidation processes (AOPs). *Chemosphere* **2022**, *308*, 136205. [CrossRef] [PubMed]
8. Mahbub, P.; Duke, M. Scalability of advanced oxidation processes (AOPs) in industrial applications: A review. *J. Environ. Manag.* **2023**, *345*, 118861. [CrossRef] [PubMed]
9. Vorontsov, A.V. Advancing Fenton and photo-Fenton water treatment through the catalyst design. *J. Hazard. Mater.* **2019**, *372*, 103–112. [CrossRef]
10. Li, N.; He, X.; Ye, J.; Dai, H.; Peng, W.; Cheng, Z.; Yan, B.; Chen, G.; Wang, S. H_2O_2 activation and contaminants removal in heterogeneous Fenton-like systems. *J. Hazard. Mater.* **2023**, *458*, 131926. [CrossRef]
11. Unal, B.O.; Bilici, Z.; Ugur, N.; Isik, Z.; Harputlu, E.; Dizge, N.; Ocakoglu, K. Adsorption and Fenton oxidation of azo dyes by magnetite nanoparticles deposited on a glass substrate. *J. Water Process Eng.* **2019**, *32*, 100897. [CrossRef]
12. Tunç, S.; Gürkan, T.; Duman, O. On-line spectrophotometric method for the determination of optimum operation parameters on the decolorization of Acid Red 66 and Direct Blue 71 from aqueous solution by Fenton process. *Chem. Eng. J.* **2012**, *181–182*, 431–442. [CrossRef]
13. Rubeenaa, K.K.; Reddy, P.H.P.; Laiju, A.R.; Nidheesh, P.V. Iron impregnated biochars as heterogeneous Fenton catalyst for the degradation of Acid Red 1 dye. *J. Environ. Manag.* **2018**, *226*, 320–332. [CrossRef]
14. Sharma, M.; Tyagi, V.V.; Chopra, K.; Kothari, R.; Singh, H.M.; Pandey, A.K. Advancement in solar energy-based technologies for sustainable treatment of textile wastewater: Reuse, recovery and current perspectives. *J. Water Process Eng.* **2023**, *56*, 104241. [CrossRef]
15. Rusevova, K.; Kopinke, F.D.; Georgi, A. Nano-sized magnetic iron oxides as catalysts for heterogeneous Fenton-like reactions-influence of Fe(II)/Fe(III) ratio on catalytic performance. *J. Hazard. Mater.* **2012**, *241–242*, 433–440. [CrossRef] [PubMed]
16. Minella, M.; Marchetti, G.; De Laurentiis, E.; Malandrino, M.; Maurino, V.; Minero, C.; Vione, D.; Hanna, K. Photo-Fenton oxidation of phenol with magnetite as iron source. *Appl. Catal. B Environ.* **2014**, *154–155*, 102–109. [CrossRef]
17. Xia, P.; Zhang, H.; Ye, Z. Recent advances in the application of natural iron and clay minerals in heterogeneous electro-Fenton process. *Curr. Opin. Electrochem.* **2024**, *46*, 101495. [CrossRef]
18. Cai, M.; Yang, H.; Yang, C.; Zhou, Y.; Wu, H. Activated sludge incineration ash derived Fenton-like catalyst: Preparation and its degradation performance of Methylene Blue. *J. Inorg. Mater.* **2024**, *39*, 1135–1142. [CrossRef]
19. Yan, J.; Yang, L.; Qian, L.; Han, L.; Chen, M. Nano-magnetite supported by biochar pyrolyzed at different temperatures as hydrogen peroxide activator: Synthesis mechanism and the effects on ethylbenzene removal. *Environ. Pollut.* **2020**, *261*, 114020. [CrossRef]
20. Kang, Y.W.; Hwang, K.Y. Effects of reaction conditions on the oxidation efficiency in the Fenton process. *Water Res.* **2000**, *34*, 2786–2790. [CrossRef]
21. Barbusiński, K.; Majewski, J. Discoloration of azo dye Acid Red 18 by Fenton reagent in the presence of iron powder. *Pol. J. Environ. Stud.* **2003**, *12*, 151–155.
22. Malakootian, M.; Moridi, A. Efficiency of electro-Fenton process in removing Acid Red 18 dye from aqueous solutions. *Process Saf. Environ. Prot.* **2017**, *111*, 138–144. [CrossRef]
23. Hassani, A.; Karaca, C.; Karaca, S.; Khataee, A.; Açisli, Ö.; Yilmaz, B. Enhanced removal of Basic Violet 10 by heterogeneous sono-Fenton process using magnetite nanoparticles. *Ultrason. Sonochem.* **2018**, *42*, 390–402. [CrossRef]
24. Wei, J.; Shen, W. FeOOH quantum dot decorated flower-like WO_3 microspheres for visible light driven photo-Fenton degradation of Methylene Blue and Acid Red-18. *Colloids Surf. A Physicochem. Eng. Asp.* **2022**, *643*, 128754. [CrossRef]
25. Kulštáková, A. Removal of pharmaceutical micropollutants from real wastewater matrices by means of photochemical advanced oxidation processes—A review. *J. Water Process Eng.* **2023**, *53*, 103727. [CrossRef]
26. Bergendahl, J.A.; Thies, T.P. Fenton's oxidation of MTBE with zero-valent iron. *Water Res.* **2004**, *38*, 327–334. [CrossRef]
27. Azizi, A.; Moghaddam, M.R.A.; Maknoon, R.; Kowsari, E. Investigation of enhanced Fenton process (EFP) in color and COD removal of wastewater containing Acid Red 18 by response surface methodology: Evaluation of EFP as post treatment. *Desalination Water Treat.* **2015**, *57*, 1944–3994. [CrossRef]
28. Garcia-Segura, S.; Brillas, E. Combustion of textile monoazo, diazo and triazo dyes by solar photoelectro-Fenton: Decolorization, kinetics and degradation routes. *Appl. Catal. B Environ.* **2016**, *181*, 681–691. [CrossRef]
29. Gharaghani, M.A.; Dehdarirad, A.; Mahdizadeh, H.; Hashemi, H.; Nasiri, A.; Samaei, M.R.; Mohammadpour, A. Photocatalytic degradation of Acid Red 18 by synthesized $AgCoFe_2O_4$@Ch/AC: Recyclable, environmentally friendly, chemically stable, and cost-effective magnetic nano hybrid catalyst. *Int. J. Biol. Macromol.* **2024**, *269*, 131897. [CrossRef]
30. Vázquez-Vélez, E.; Martínez, H.; Castillo, F. Degradation of Acid Red 1 catalyzed by peroxidase activity of iron oxide nanoparticles and detected by SERS. *Nanomaterials* **2021**, *11*, 3044. [CrossRef]
31. Ara, A.; Khattak, R.; Khan, M.S.; Begum, B.; Khan, S.; Han, C. Synthesis, characterization, and solar photo-activation of chitosan-modified nickel magnetite bio-composite for degradation of recalcitrant organic pollutants in water. *Catalysts* **2022**, *12*, 983. [CrossRef]

32. Hassan, H.; Hameed, B.H. Oxidative decolorization of Acid Red 1 solutions by Fe-zeolite Y type catalyst. *Desalination* **2011**, *276*, 45–52. [CrossRef]
33. Zare, M.R.; Mengelizadeh, N.; Aghdavodian, G.; Zare, F.; Ansari, Z.; Hashemi, F.; Moradalizadeh, S. Adsorption of Acid Red 18 from aqueous solutions by GO-COFe$_2$O$_4$: Adsorption kinetic and isotherms, adsorption mechanism and adsorbent regeneration. *Desalination Water Treat.* **2024**, *317*, 100219. [CrossRef]
34. Santana, C.S.; Ramos, M.D.N.; Velloso, C.C.V.; Aguiar, A. Kinetic evaluation of dye decolorization by Fenton processes in the presence of 3-Hydroxyanthranilic Acid. *Int. J. Environ. Res. Public Health* **2019**, *16*, 1602. [CrossRef] [PubMed]
35. Liang, X.; Zhong, Y.; Zhu, S.; Zhu, J.; Yuan, P.; He, H.; Zhang, J. The decolorization of Acid Orange II in non-homogeneous Fenton reaction catalyzed by natural vanadium–titanium magnetite. *J. Hazard. Mater.* **2010**, *181*, 112–120. [CrossRef]
36. Zhao, Q.; Zhang, C.; Tong, X.; Zou, Y.; Li, Y.; Wei, F. Fe$_3$O$_4$-NPs/orange peel composite as magnetic heterogeneous Fenton-like catalyst towards high-efficiency degradation of methyl orange. *Water Sci. Technol.* **2021**, *84*, 159–171. [CrossRef]
37. Nguyen, X.S.; Ngo, K.D. The role of metal-doped into magnetite catalysts for the photo-Fenton degradation of organic pollutants. *J. Surf. Eng. Mater. Adv. Technol.* **2018**, *8*, 1–14. [CrossRef]
38. Choe, Y.J.; Kim, J.; Byun, J.Y.; Kim, S.H. An electro-Fenton system with magnetite coated stainless steel mesh as cathode. *Catal. Today* **2021**, *359*, 16–22. [CrossRef]
39. Abou-Gamra, Z.M. Kinetic and thermodynamic study for Fenton-like oxidation of Amaranth Red dye. *Adv. Chem. Eng. Sci.* **2014**, *4*, 285–291. [CrossRef]
40. Shuchi, S.B.; Suhan, M.B.K.; Humayun, S.B.; Haque, M.E.; Islam, M.S. Heat-activated potassium persulfate treatment of Sudan Black B dye: Degradation kinetic and thermodynamic studies. *J. Water Process Eng.* **2021**, *39*, 101690. [CrossRef]
41. Ball, P.; Nicholls, C.H. Azo-hydrazone tautomerism of hydroxyazo compounds—A review. *Dyes Pigment.* **1982**, *3*, 5–26. [CrossRef]
42. Omura, T.; Kayane, Y.; Tezuka, Y. Design of chlorine-fast reactive dyes: Part 1: The role of sulphonate groups and optimization of their positions in an arylazonaphthol system. *Dyes Pigment.* **1992**, *20*, 227–246. [CrossRef]
43. Zhang, G.; Zhang, S. Quantitative structure-activity relationship in the photodegradation of azo dyes. *J. Environ. Sci.* **2020**, *90*, 41–50. [CrossRef] [PubMed]
44. Pearson, R.G. Hard and soft acids and bases. *J. Am. Chem. Soc.* **1963**, *85*, 3533–3539. [CrossRef]
45. Dai, H.; Xu, S.; Chen, J.; Miao, X.; Zhu, J. Oxalate enhanced degradation of Orange II in heterogeneous UV-Fenton system catalyzed by Fe$_3$O$_4$@g-Fe$_2$O$_3$ composite. *Chemosphere* **2018**, *199*, 147–153. [CrossRef]
46. Paz, C.B.; Araújo, R.S.; Oton, L.F.; Oliveira, A.C.; Soares, J.M.; Medeiros, S.N.; Rodríguez-Castellón, E.; Rodríguez-Aguado, E. Acid Red 66 dye removal from aqueous solution by Fe/C-based composites: Adsorption, kinetics and thermodynamic studies. *Materials* **2020**, *13*, 1107. [CrossRef] [PubMed]
47. Gurushankar, K.; Chinnaiah, K.; Kannan, K.; Gohulkumar, M.; Periyasamy, P. Synthesis and characterization of FeO nanoparticles by hydrothermal method. *Rasayan J. Chem.* **2021**, *14*, 1985–1989. [CrossRef]
48. Martina, M.R.; Zoli, L.; Sani, E. Synthesis and characterization of goethite (α-FeOOH) magnetic nanofluids. *Int. J. Thermofluids* **2022**, *15*, 100169. [CrossRef]
49. Abo-Farha, S.A. Comparative study of oxidation of some azo dyes by different advanced oxidation processes: Fenton, Fenton-Like, photo-Fenton and photo-Fenton-like. *J. Am. Sci.* **2010**, *6*, 128–142.
50. Chen, K.; Wang, G.; Li, W.; Wan, D.; Hu, Q.; Lu, L. Application of response surface methodology for optimization of Orange II removal by heterogeneous Fenton-like process using Fe$_3$O$_4$ nanoparticles. *Chin. Chem. Lett.* **2014**, *25*, 1455–1460. [CrossRef]
51. Quiñones-Murillo, D.H.; Ariza-Reyes, A.A.; Ardila-Vélez, L.J. Some kinetic and synergistic considerations on the oxidation of the azo compound Ponceau 4R by solar–mediated heterogeneous photocatalytic ozonation. *Desalination Water Treat.* **2019**, *170*, 61–74. [CrossRef]
52. Lucas, M.S.; Algarra, M.; Jiménez-Jiménez, J.; Rodríguez-Castellón, E.; Peres, J.A. Catalytic activity of porous phosphate heterostructures-Fe towards Reactive Black 5 degradation. *Int. J. Photoenergy* **2013**, *2013*, 658231. [CrossRef]
53. Fu, F.; Wang, Q.; Tang, B. Effective degradation of C.I. Acid Red 73 by advanced Fenton process. *J. Hazard. Mater.* **2010**, *174*, 17–22. [CrossRef] [PubMed]
54. Faria, A.J.M.; Silva, A.N.; Oliveira, A.C.; do Carmo, J.V.C.; Saraiva, G.D.; Juca, R.F.; Morales, M.A.; Lang, R.; Jiménez, J.J.; Rodríguez-Castellón, E. Catalytic performances of the nano FeCo solids for biofuel additives production: Incorporation of promoters effects on the stability of the catalysts. *Energy Fuels* **2023**, *37*, 17328–17344. [CrossRef]
55. Rajan, A.; Sharma, M.; Sahu, N.S. Assessing magnetic and inductive thermal properties of various surfactants functionalised Fe$_3$O$_4$ nanoparticles for hyperthermia. *Sci. Rep.* **2020**, *10*, 15045. [CrossRef]
56. Zhong, Y.; Yu, L.; Chen, Z.-F.; He, H.; Ye, F.; Cheng, G.; Zha, Q. Microwave-assisted synthesis of Fe$_3$O$_4$ nanocrystals with predominantly exposed facets and their heterogeneous UVA/Fenton catalytic activity. *ACS Appl. Mater. Interfaces* **2017**, *9*, 29203–29212. [CrossRef] [PubMed]
57. Ai, Q.; Yuan, Z.; Huang, R.; Yang, C.; Jiang, G.; Xiong, J.; Huang, Z.; Yuan, S. One-pot co-precipitation synthesis of Fe$_3$O$_4$ nanoparticles embedded in 3D carbonaceous matrix as anode for lithium ion batteries. *J. Mater. Sci.* **2019**, *54*, 4212–4224. [CrossRef]
58. Yamashita, T.; Hayes, P. Analysis of XPS spectra of Fe^{2+} and Fe^{3+} ions in oxide materials. *Appl. Surf. Sci.* **2008**, *254*, 2441–2449. [CrossRef]

59. Konstantinou, I.K.; Albanis, T.A. TiO_2-assisted photocatalytic degradation of azo dyes in aqueous solution: Kinetic and mechanistic investigations: A review. *Appl. Catal. B Environ.* **2004**, *49*, 1–14. [CrossRef]
60. Yin, Z.; Zhang, K.; Ma, N.; Liu, X.; Yin, Z.; Wang, H.; Yang, X.; Wang, Y.; Qin, X.; Cheng, D.; et al. Catalytic membrane electrode with Co_3O_4 nanoarrays for simultaneous recovery of water and generation of hydrogen from wastewater. *Sci. China Mater.* **2023**, *66*, 651–663. [CrossRef]
61. Chowdhury, A.P.; Anantharaju, K.S.; Keshavamurthy, K.; Rokhum, S.L. Recent advances in efficient photocatalytic degradation approaches for azo dyes. *J. Chem.* **2023**, *2023*, 9780955. [CrossRef]
62. Klassen, N.V.; Marchington, D.; McGowan, H.C.E. H_2O_2 determination by the I_3^- method and by $KMnO_4$ titration. *Anal. Chem.* **1994**, *66*, 2921–2925. [CrossRef]
63. Liu, X.; Zhao, T.; Liu, P.; Cui, P.; Hu, P. Manufacture of nano graphite oxides derived from aqueous glucose solutions and in-situ synthesis of magnetite graphite oxide composites. *Mater. Chem. Phys.* **2015**, *153*, 202–208. [CrossRef]
64. Hashemian, S. Fenton-like oxidation of Malachite Green solutions: Kinetic and thermodynamic study. *J. Chem.* **2013**, *2013*, 809318. [CrossRef]